Synthesis and characterization of the oxygen-deficient perovskite $BaFe_{0.9-x}Y_{0.1}Co_xO_{3-\delta}$ ($0 \leq x \leq 0.15$)

A. S. Urusova[1], A.V. Bryuzgina[1], V. A Cherepanov[1,*], P. D. Battle[2], and C-M. Chin[2],

1. Institute of Natural Sciences, Ural Federal University, Lenin av., 51, Yekaterinburg, 620000, Russia

2. Inorganic Chemistry Laboratory, University of Oxford, South Parks Road, Oxford, OX1 3QR, U. K.

Abstract

$BaFe_{0.9-x}Y_{0.1}Co_xO_{3-\delta}$ ($0 \leq x \leq 0.15$) is shown to adopt the cubic perovskite structure at temperatures up to 1400 K in air. The oxygen vacancy concentration increases with both cobalt content and temperature, with $BaFe_{0.75}Y_{0.1}Co_{0.15}O_{2.35}$ being the most oxygen-deficient composition observed. At 700 K the conductivity is ~2 S cm^{-1} across the whole composition range. Measurements of the Seebeck coefficient show that holes are the dominant carrier. The coefficient of thermal expansion is essentially constant above 800 K, but not at lower temperatures. Chemical reactivity tests, along with the coefficient of expansion, show that these perovskites would not be suitable electrodes for fuel cells with fluorite electrolytes but they might serve as permeable membranes in catalytic reactors.

Introduction

The electrodes of a solid-oxide fuel cell must possess a number of properties. In order to connect to the external circuit they must have a good electronic conductivity, whereas in order to connect to the solid electrolyte they must have a good ionic conductivity. They must not react chemically with the electrolyte at the proposed operating temperature and $p(O_2)$ of the cell, nor should they decompose under those conditions. In order to avoid cracking, their coefficient of thermal expansion must be compatible with that of the electrolyte. Finally, they should catalyse the solid/gas reactions that take place at their surface. This is a demanding list and many oxides have

been assessed and found wanting. Mixed-metal oxides with perovskite-related crystal structures have been among the more successful candidates [1]. Transition metals occupying the six-coordinate site in this structure are able to adopt mixed-valence states that often lead to electronic conductivity. Furthermore, the anion sublattice is able to tolerate high vacancy concentrations that are compatible with a high oxide-ion conductivity. Thermal expansion is difficult to predict quantitatively for a defect-rich solid and although transition-metal cations are often associated with catalytic activity it is again difficult to predict the behavior of a particular compound. It has therefore been necessary to adopt a somewhat empirical approach in the search for new electrode materials, although perovskites containing iron or cobalt have often been to the fore because these two elements undergo an extensive redox chemistry between the oxidation states +2, +3 and +4, with mixed-valence states being common [2-6]. If a perovskite-related oxide is anion deficient there is a tendency for the vacancies to adopt an ordered arrangement, either locally or in a periodic manner, with the latter scenario leading to, for example, the brownmillerite structure. This long-range ordering of vacancies tends to inhibit conductivity on the oxide sublattice and it is therefore interesting to note that Parras *et al* [7] have shown that no such ordering occurs in the $BaFe_{0.9}Y_{0.1}O_{3-\delta}$ system, and that simple cubic symmetry is maintained over a wide range of δ values. Lomakov *et al* [8] subsequently showed that $BaCo_{0.9}Y_{0.1}O_{3-\delta}$ shows the same behaviour, and this system has subsequently been investigated further by Urusova *et al* [9]. Oxide-ion transport in the $BaFe_{1-x}Y_xO_{3-\delta}$ system has been studied by Liu *et al* [10] with a view to using the material as an oxygen-separation membrane in a catalytic reactor. They concluded that it was a promising material but noted that the presence of yttrium, necessary to give structural stability, reduced the oxygen permeability to values within the range 0.4 – 0.8 $ml \cdot cm^{-2} \cdot min^{-1}$ [10].

We have now begun to explore the mixed iron/cobalt system $BaFe_{0.9-x}Y_{0.1}Co_xO_{3-\delta}$ in order to establish the composition and temperature range over which it is stable as a simple cubic perovskite, that is the (x, T) range over which it is most likely to be a good ionic conductor and where it might therefore serve as a fuel-cell component or as a membrane in a catalytic converter. We have also measured the thermal expansion coefficient and the compatibility of this compound with potential electrolyte materials. We use our results to identify the likely oxidation states of the participating transition-metal cations. We also report, briefly, our unsuccessful attempts to prepare $BaFe_{0.9-x}Y_{0.1}Me_xO_{3-\delta}$ (Me= Ni, Cu).

Experimental

Polycrystalline samples of $BaFe_{0.9-x}Y_{0.1}Me_xO_{3-\delta}$ (Me=Co, Ni, Cu) with $0.0 \leq x \leq 0.2$ were prepared using both a conventional solid state reaction route and a glycerol–nitrate technique. Yttrium(III) oxide with a purity of not less than 99.99%, barium carbonate (special purity grade), iron(III) oxide, cobalt(II,III) oxide, nickel(II) oxide and copper(II) oxide (either analytical grade or special-purity grade), metallic cobalt, metallic nickel and iron(II) oxalate dihydrate (analytical grade) were used as starting materials. In syntheses based on the solid state reaction route, the appropriate oxides and barium carbonate were mixed in the correct ratio to produce the desired composition, ground in an agate mortar under alcohol and then fired repeatedly within the temperature range 1123 – 1373 K. When using the glycerol-nitrate technique, yttrium(III) oxide, barium carbonate, iron(II) oxalate dihydrate and either metallic cobalt, metallic nickel or copper(II) oxide were dissolved in hot 4.5 M nitric acid, then the quantity of glycerol needed to completely reduce the nitrate groups was added. The solution was then dried to form a viscous gel and subsequently a brown powder. Whichever method was used, the final anneal was always performed at 1373 K in air for 100-120 h with intermediate grindings, followed by slow cooling to room temperature at the rate of ~100 K h^{-1}.

The phase composition of the reaction products was monitored by X-ray powder diffraction (XRD) with a DRON-6 diffractometer or an Inel Equinox 3000 using Cu-Kα radiation. Data were collected over the angular range $10 \leq 2\theta/° \leq 90$. The values of the unit cell parameters were calculated using the "Celref 3" package and the structural parameters were refined using the Fullprof program suite [11]. In selected cases the temperature dependence of the crystal structure was studied by *in situ* high-temperature X-ray diffraction over the temperature range 298 < T/K < 1273 K in air.

The average oxidation state of the transition-metal cations in $BaFe_{0.9-x}Y_{0.1}Co_xO_{3-\delta}$ ($0 \leq x \leq 0.15$) was determined by iodometric titration and hence the oxygen content of each sample was determined. The samples, weighing 0.1–0.2 g, were dissolved in dilute hydrochloric acid in the presence of KI and then titrated against a thiosulfate solution that had been standardized by a chromatometric titration against $K_2Cr_2O_7$ [9]. In all cases the end points were obtained using an automatic titration device (Akvilon ATP-02). The use of simple iron oxide standards showed that the accuracy of the oxygen content determination was not less than ±0.04. For two samples, the oxygen content was also determined by reducing the sample inside an STA 409PC (Netzsch Gmbh) thermogravimetric analyser (TGA) in a flow of dried 10 vol. % H_2–90 vol. % Ar gas at 1373 K for 10 hours. The reduction products were BaO, Y_2O_3, Fe and Co. The accuracy of the oxygen-content determination by TGA was not less than ±0.01. Having established that the two analytical methods gave consistent results, the temperature dependence of the oxygen content of the single-phase oxides was then determined by TGA, in air, over the temperature range 298

<T/K < 1373 using both dynamic (heating/cooling rate of 2 K min^{-1}) and static methods (stepwise heating/cooling before holding at constant temperature for 8 h).

The temperature dependence of the molar magnetic susceptibility of $BaFe_{0.9-x}Y_{0.1}Co_xO_{3-\delta}$ (x = 0.0, 0.1 and 0.15) was measured using a SQUID magnetometer. Measurements were made while warming the sample through the temperature range $5 \leq T/K \leq 300$ after it had been cooled in zero field (ZFC) and also after cooling it in the measuring field of 100 Oe (FC).

The temperature dependence of the thermal expansion of the reaction products was measured in air over the temperature range 298 < T/K < 1373 K with a heating/cooling rate of 5 K min^{-1} using a high-temperature dilatometer (DIL 402 C Netzsch GmbH). Dense specimens of $BaFe_{0.9-x}Y_{0.1}Co_xO_{3-\delta}$ ($0 \leq x \leq 0.15$) in the form of 2x2x15 mm bars were obtained by pressing and sintering at 1473 K in air for 20 h, followed by cooling at a rate of 1.5 K min^{-1}. The density of the polished ceramic samples was not less than 90% of the theoretical value calculated from the XRD data.

Similar specimens were used for the electrical conductivity and Seebeck coefficient measurements which were performed simultaneously in the same cell. Conductivity measurements were made using a standard 4-probe DC method. The temperature dependence of the conductivity was measured in dynamic mode (heating/cooling rate ~200 $K \cdot h^{-1}$) and several points were also obtained in static mode (stepwise heating/cooling before holding at constant temperature for 1 h). The temperature difference between the two ends of the sample during measurements of the thermoelectric voltage was ~10 K.

Chemical compatibility with the electrolyte materials $Zr_{0.85}Y_{0.15}O_{2-\delta}$ and $Ce_{0.8}Sm_{0.2}O_{2-\delta}$ over the temperature range 1173–1373 K was established by mixing the electrolyte and the perovskite in a 1:1 ratio, by weight, annealing the mixture for 24 h in air and then recording the XRD pattern of the resulting material.

Results and Discusssion

The results of the characterization experiments described above were independent of the synthesis method used for each sample, demonstrating that they were equilibrium phases.

XRD analysis of a sample of $BaFe_{0.9}Y_{0.1}O_{3-\delta}$ that had been slowly cooled from 1373 K to room temperature in air showed the formation of a single, perovskite-like phase. TGA showed the composition at 298 K in air to be $BaFe_{0.9}Y_{0.1}O_{2.62}$, which is very close to that reported previously [3]. The XRD pattern of our sample was indexed in a cubic unit cell (S.G. *Pm3m*): the results of a Rietveld [12] analysis of the pattern are shown in Figure 1. Our high-temperature X-ray data showed that $BaFe_{0.9}Y_{0.1}O_{3-\delta}$ remains cubic in air at temperatures up to 1273 K.

In order to check the possibility of partial replacement of iron in the cubic solid solution a number of samples with the overall composition $BaFe_{0.9-x}Y_{0.1}Me_xO_{3-\delta}$ (Me=Co, Ni, Cu) with $0.0 \leq x \leq 0.2$ were prepared using a solid state reaction route and the glycerol–nitrate technique. XRD showed that for slowly-cooled Co-containing samples, a single-phase $BaFe_{0.9-x}Y_{0.1}Co_xO_{3-\delta}$ solid solution formed in air over the composition range $0 \leq x \leq 0.15$. Beyond this range, the major impurity phase was $BaCoO_{3-\delta}$, see Figure 2. The substitution of nickel or copper for iron did not lead to the formation of solid solutions under the conditions used in this investigation. The $BaFe_{0.9-x}Y_{0.1}Ni_xO_{3-\delta}$ sample with $x=0.1$ consisted of three phases: $BaFe_{0.9}Y_{0.1}O_{3-\delta}$, $YBa_3Fe_2O_8$ and NiO. The Cu-containing samples $BaFe_{0.9-x}Y_{0.1}Cu_xO_{3-\delta}$ with $0.0 \leq x \leq 0.2$ also consisted of three phases: $BaFe_{0.9}Y_{0.1}O_{3-\delta}$, $BaCuY_2O_5$ and $BaCu_2O_3$.

As in the case of $BaFe_{0.9}Y_{0.1}O_{3-\delta}$, the crystal structure of all single-phase samples in the solid solution $BaFe_{0.9-x}Y_{0.1}Co_xO_{3-\delta}$ ($0 \leq x \leq 0.15$) could be described in a cubic unit cell (S.G. *Pm3m*). For example, the results of a Rietveld analysis of the XRD pattern of $BaFe_{0.8}Y_{0.1}Co_{0.1}O_{3-\delta}$, are shown in Figure 3. The unit cell parameters and oxygen content at room temperature for all single-phase samples are listed in Table 1. The ionic radii of cobalt ($r_{Co^{3+}/Co^{4+}}$ = 0.75/0.67 Å, CN=6) are less than those of iron ($r_{Fe^{3+}/Fe^{4+}}$ = 0.785/0.725 Å, CN=6) and the substitution of cobalt for iron consequently leads to a monotonous decrease of the unit cell parameter and hence to a decrease in the average B-O bond length, see Figure 4, which varies linearly between 2.045 and 2.039 Å as the cobalt content increases. These values can be compared with the values of 2.059, 2.053 and 2.216 Å found for the mean high-spin Fe^{3+} – O, high-spin Co^{3+} – O and Y^{3+} – O bond lengths at the six-coordinate sites in $Sr_2Fe_2O_5$, $Sr_2Co_2O_5$ and Ba_2YRuO_6, respectively[13-15]. The Y^{3+} cation is clearly larger than the others but there is no evidence to suggest that ionic size limits the extent to which Fe^{3+} can be replaced by Co^{3+} when the yttrium content is held constant. It is more likely that the maximum value of x is determined by the thermodynamics of $BaCoO_{3-\delta}$ formation.

Figure 5 shows the variation of the unit cell parameter and the oxygen content, determined by TGA, of $BaFe_{0.8}Y_{0.1}Co_{0.1}O_{3-\delta}$ with increasing temperature in air (Po_2 = 0.21 atm); the structure remains cubic up to 1273 K. Figure 6 shows the temperature variation of the oxygen content for samples having different cobalt contents. The oxygen content increases as the temperature decreases and mass saturation occurs at $T<630$ K upon cooling. Solid lines represent data obtained in dynamic measurements (cooling rate 2 K min^{-1}) and points correspond to values obtained in static measurements (isothermal dwells for 8 h). The excellent agreement between the data obtained by the different methods suggest that the oxygen exchange process and, hence equilibration between the solid oxides and gaseous phase is fast, at least in the case of for

$BaFe_{0.75}Y_{0.1}Co_{0.15}O_{3-\delta}$. The substitution of cobalt for iron results in a decrease in oxygen content at all temperatures. The average oxidation state of the transition metal cations at 1400 K decreases from ~2.90 for x = 0.0 to 2.64 for x = 0.15, reflecting the relative ease of reduction of the trivalent cation in the case of cobalt compared to iron. This is consistent with the fact that cobalt is more electronegative than iron (χ_{Co} = 1.88; χ_{Fe} = 1.83 on the Pauling scale). With the assumption that all the cobalt ions serve as electron traps and are reduced to Co^{2+} state, then the chemical formula for x = 0.15 at 1400 K can be written as $BaFe^{3+}_{0.576}Fe^{2+}_{0.174}Y_{0.1}Co^{2+}_{0.15}O_{2.338}$, with an average oxidation state for iron of 2.77.

The temperature dependence of the electrical conductivity and the Seebeck coefficient of compositions having x = 0.0 and 0.15 is shown in Figure 7. Both quantities vary smoothly between room temperature and 630 K, the temperature at which oxygen loss begins, see Figure 6. In this region the concentration of charge carriers is constant but their mobility increases. The conductivity of the Co-free sample $BaFe_{0.9}Y_{0.1}O_{3-\delta}$ shows some hysteresis in the temperature region where oxygen loss begins; the heating curve is higher than cooling curve, see Figure 7. In contrast, no hysteresis is apparent in the temperature dependence of the conductivity $BaFe_{0.75}Y_{0.1}Co_{0.15}O_{3-\delta}$, suggesting that this composition, with a higher concentration of anion vacancies, can undergo a higher rate of oxygen exchange than $BaFe_{0.9}Y_{0.1}O_{3-\delta}$. The positive Seebeck coefficient demonstrates that the charge carriers are holes. We propose that these are localized on Fe^{4+} cations, which must be present when $(3-\delta) > 2.5$. When the oxygen content drops below 2.5 the mean oxidation state of iron will depend on the concentration of cobalt. In the case of the most Co-rich composition, x = 0.15, samples with an oxygen content $2.425 < (3-\delta) < 2.5$ might be considered to contain Fe^{3+} and Co^{3+}/Co^{2+}. At lower oxygen contents the average oxidation state of iron must drop below +3. However, our Seebeck data demonstrate that holes remain the principal charge carriers across the whole composition range, thus suggesting that Fe^{4+} is always present. Previous accounts of electrical transport in closely related compositions [16-18] have considered the disproportionation reaction

$$2Fe^{3+} = Fe^{4+} + Fe^{2+} \qquad (1)$$

to play a key role in carrier generation. It seems likely that this mechanism is also important for the creation of holes in the $BaFe_{0.9-x}Y_{0.1}Co_xO_{3-\delta}$ system. However, further work will be necessary in order to resolve this issue unambiguously. The enhanced conductivity of the Co-containing sample suggests that the cobalt cations decrease the hopping activation energy and therefore slightly increase the conductivity in comparison to that of the undoped oxide.

The temperature dependence of the inverse molar magnetic susceptibility of the samples having x = 0.05 and 0.15 is shown in Figure 8; the data for the sample with x = 0.0 are qualitatively very

similar to those measured for x = 0.05. The values of the effective magnetic moment (μ_{eff}) and the Weiss constant (θ) obtained by fitting the data collected above 150 K to the Curie-Weiss law are listed in Table 2. The mean oxidation state of the iron in $BaFe_{0.9}Y_{0.1}O_{2.62}$ is +3.26. The formula can therefore be written $BaFe^{3+}_{0.64}Fe^{4+}_{0.26}Y_{0.1}O_{2.62}$. The unit cell parameter, see Table 1, is consistent with the presence on the six-coordinate site of a disordered arrangement of high-spin iron and yttrium. However, the effective magnetic moment is too low to be consistent with this model. If significant short-range magnetic ordering is present at room temperature it will render μ_{eff} values derived from the Curie-Weiss law meaningless. The presence of such ordering is highly likely, given that many other Fe^{3+} oxides order antiferromagnetically above room temperature. The unfortunate consequence of this is that we are unable to use our magnetic data to confirm assignments of spin-state and oxidation state in these compositions. The data presented in Figure 8 suggest that each composition undergoes a transition to a spin-glass phase at ~30 K, but a detailed discussion of this behavior is beyond the scope of the present study. The absence of hysteresis at the highest temperature measured demonstrates that our samples are not contaminated by magnetic impurities.

The thermal expansion of $BaFe_{0.9-x}Y_{0.1}Co_xO_{3-\delta}$ ceramics over the temperature range 298 – 1400 K in air is shown in Figure 9. All the thermal expansion curves of compositions in the solid solution $BaFe_{0.9-x}Y_{0.1}Co_xO_{3-\delta}$ have a nonlinear form. For example, from room temperature to ~473 K the thermal expansion coefficient (TEC) of $BaFe_{0.8}Y_{0.1}Co_{0.1}O_{3-\delta}$ was found to decrease to zero with increasing temperature. It then increases, reaching a maximum at 757 K. The nonlinearity is also seen in the values of the unit cell parameters deduced from our X-ray data, see Figure 5. The effect is small and is unlikely to be caused by a spin-state transition. A change in the degree of local vacancy ordering is perhaps more likely. ^{57}Fe Mössbauer spectroscopy might be able to resolve this issue in the future. The average expansion coefficient over the 1050 K temperature range measured is ~2.32×10^{-5} K^{-1}; the value determined from the temperature dependence of the unit cell parameter, see Figure 5, is 2.52×10^{-5} K^{-1}. These values are large but not atypical for oxygen-deficient perovskites in which the increase in cation radius that accompanies the loss of oxygen augments the expansion due to thermal vibrations [19-21].

In order to investigate what chemical interactions might occur between these perovskites and the electrolyte in a fuel cell, $BaFe_{0.9-x}Y_{0.1}Co_xO_{3-\delta}$ (x=0, 0.05, 0.1, 0.15) samples were mixed with the solid-electrolyte materials $Ce_{0.8}Sm_{0.2}O_{2-\delta}$ and $Zr_{0.85}Y_{0.15}O_{2-\delta}$ in mass ratio 1 : 1 and fired for 24 h at 1073 K, 1173 K, 1273 K and 1373 K in air. It was found that $BaFe_{0.9-x}Y_{0.1}Co_xO_{3-\delta}$ is chemically inert to $Ce_{0.8}Sm_{0.2}O_{2-\delta}$ over the temperature range studied. On the contrary, $Zr_{0.85}Y_{0.15}O_{2-\delta}$ reacted with all the perovskite materials, even at 1173 K, forming the insulator

barium zirconate $BaZrO_3$. Figure 10 illustrates shows the post-firing XRD patterns of the two of the mixtures.

Conclusion

We have shown that $BaFe_{0.9-x}Y_{0.1}Me_xO_{3-\delta}$ (Me=Co, Ni, Cu) can be synthesized as a simple cubic perovskite for x = Co for $x \leq 0.15$ by either a sol-gel route or a solid-state route. The X-ray diffraction patterns of samples in that composition range showed no evidence of long-range ordering of the vacancies on the anion sublattice. For all $x \leq 0.15$ the perovskite structure shows stability throughout the temperature range relevant to solid-oxide fuel cells despite the fact that oxide ions are readily removed from within the structure, see Figure 6. Unfortunately, a number of factors mitigate against the use of $BaFe_{0.9-x}Y_{0.1}Co_xO_{3-\delta}$ as an electrode in fuel cells. Firstly, the conductivity, see Figure 7, is much lower than those of viable materials [22]. The unusual temperature variation of the coefficient of thermal expansion might also limit the usefulness of these compositions and it is clear, see Figure 10, that their reactivity will preclude their use with yttrium-stabilized zirconia electrolytes. They are chemically compatible with $Ce_{1-y}Sm_yO_{2-\delta}$ but this electrolyte has a thermal expansion coefficient of only 8-10 x 10^{-6} K^{-1} between room temperature and 1000 °C [23], approximately half the value found for $BaFe_{0.9-x}Y_{0.1}Co_xO_{3-\delta}$. Although it might be possible to overcome this problem by using a composite cathode, it seems unlikely that $BaFe_{0.9-x}Y_{0.1}Co_xO_{3-\delta}$ will find applications in fuel cells in the foreseeable future. However, as was pointed out by Liu *et al* [10], the potential of the Ba-Y-Fe-O system as a membrane material would be enhanced if the oxygen permeability could be increased. $BaFe_{0.9-x}Y_{0.1}Co_xO_{3-\delta}$ has a higher concentration of anion vacancies than the cobalt-free system and the use of this material would therefore be expected to increase the membrane permeability. Thus, although it would be necessary to balance the improvement in performance against issues of cost and toxicity, $BaFe_{0.9-x}Y_{0.1}Co_xO_{3-\delta}$ might prove to a better membrane material than $BaFe_{1-x}Y_xO_{3-\delta}$.

Acknowledgments

This work was supported in part by the Ministry of Education and Science of RF (State Task project No 1039) and by Act 211 Government of the Russian Federation, agreement No 02.A03.21.0006.

References

1. A. J. Jacobson, *Chem. Mater.* **22**, 660 (2010)
2. P. D. Battle and T. C. Gibb, *J. Chem. Soc. Dalton Trans.* 667 (1987)
3. P. D. Battle, T. C. Gibb and A. T. Steel, *J. Chem. Soc. Dalton Trans.* 83 (1988)
4. T. C. Gibb, *Journal of the Chemical Society-Dalton Transactions* 1455-1470 (1985)
5. T. C. Gibb, *Journal of the Chemical Society-Dalton Transactions* 1419-1423 (1987)
6. T. C. Gibb and M. Matsuo, *Journal of Solid State Chemistry* **81**, 83-95 (1989)
7. M. Parras, E. Garcia, J. M. Gonzalez-Calbet and M. Vallet-Regi, *J. Less-Common Metals* **169**, 25 (1991)
8. M. V. Lomakov, S. Y. Istomin, A. M. Abakumov, G. V. Tendeloo and E. V. Antipov, *Solid State Ionics* **179**, 1885 (2008)
9. A. S. Urusova, V. A. Cherepanov, T. V. Aksenova, L. Y. Gavrilova and E. A. Kiselev, *J. Solid State Chem.* **202**, 207 (2013)
10. X. Liu, H. Zhao, J. Yang, Y. Li, T. Chen, X. Lu, W. Ding and F. Li, *J. Membrane Science* **383**, 235 (2011)
11. J. Rodriguez-Carvajal, *Physica B* **192**, 55 (1993)
12. H. M. Rietveld, *Journal of Applied Crystallography* **2**, 65 (1969)
13. P. D. Battle and C. W. Jones, *J. Solid State Chem.* **78**, 108 (1989)
14. J. E. Auckett, A. J. Studer, N. Sharma and C. D. Ling, *Solid State Ionics* **225**, 432 (2012)
15. E. Sullivan, J. Hadermann and C. Greaves, *J. Solid State Chem.* **184**, 649 (2011)
16. J. Mizusaki, T. Sasamoto, W. R. Cannon and H. K. Bowen, *J. Am. Ceram. Soc.* **65**, 363 (1982)
17. J. Mizusaki, T. Sasamoto, W. R. Cannon and H. K. Bowen, *J. Am. Ceram. Soc.* **66**, 247 (1983)
18. J. Mizusaki, M. Yoshihiro, S. Yamauchi and K. Fueki, *J. Solid State Chem.* **58**, 257 (1985)
19. F. Dong, D. Chen, Y. Chen, Q. Zhao and Z. Shao, *Journal of Materials Chemistry* **22**, 15071-15079 (2012)
20. Y. Lu, H. Zhao, X. Cheng, Y. Jia, X. Du, M. Fang, Z. Du, K. Zheng and K. Swierczek, *Journal of Materials Chemistry A* **3**, 6202-6214 (2015)
21. L. Yan, H. Ding, Z. Zhu and X. Xue, *Journal of Power Sources* **196**, 9352-9355 (2011)
22. S. Hou, J. A. Alonso, S. Rajasekhara, M. J. Martinez-Lope, M. T. Fernandez-Diaz and J. B. Goodenough, *Chem. Mater.* **22**, 1071 (2010)
23. W. Huang, P. Shuk and M. Greenblatt, *Solid State Ionics* **100**, 23 (1997)

Table 1 Structural parameters and oxygen content at room temperature for compositions in the solid solution $BaFe_{0.9-x}Y_{0.1}Co_xO_{3-\delta}$

x	*a*, Å	*V*, $(Å)^3$	Oxygen content (3-δ)
0.00	4.090(1)	68.41(3)	2.62[*] 2.60[**] 2.59[3]
0.05	4.086(1)	68.20(1)	2.57[**]
0.10	4.081(1)	67.97(1)	2.55[*] 2.53[**]
0.15	4.078(3)	67.81(4)	2.51[**]

Space group *Pm3m*, Ba (0.5; 0.5; 0.5), Fe/Y/Co (0; 0; 0), O (0.5;0;0)
[*] data obtained by TGA
[**] data obtained by titration method

Table 2 Curie-Weiss parameters of $BaFe_{0.9-x}Y_{0.1}Co_xO_{3-\delta}$

x	μ_{eff}, μ_B	θ, K
0	3.73(2)	-100(2)
0.05	3.71(2)	-90(2)
0.15	3.97(1)	-214(1)

Figure Captions

Figure 1 Observed (points) and calculated (solid line) room-temperature X-ray diffraction patterns of $BaFe_{0.9}Y_{0.1}O_{2.61}$. A difference curve is plotted at the bottom. Vertical marks represent the position of allowed Bragg reflections.

Figure 2 Observed (points) and calculated (solid line) room-temperature X-ray diffraction patterns of $BaFe_{0.7}Y_{0.1}Co_{0.2}O_{3-\delta}$. The positions of reflections from the perovskite and two potential impurity phases are marked.

Figure 3 Observed (points) and calculated (solid line) room-temperature X-ray diffraction patterns of $BaFe_{0.8}Y_{0.1}Co_{0.1}O_{3-\delta}$. A difference curve is plotted at the bottom. Vertical marks represent the position of allowed Bragg reflections.

Figure 4 The room-temperature unit cell parameter of $BaFe_{0.9-x}Y_{0.1}Co_xO_{3-\delta}$ as a function of cobalt content.

Figure 5 The unit cell parameters and values of the oxygen content in $BaFe_{0.8}Y_{0.1}Co_{0.1}O_{3-\delta}$ as a function of temperature, measured in air.

Figure 6 Temperature dependence of oxygen content, measured in air by TGA, in $BaFe_{0.9-x}Y_{0.1}Co_xO_{3-\delta}$ ($0 \leq x \leq 0.15$)

Figure 7 Temperature dependence of (a) the electrical conductivity and (b) the Seebeck coefficient of $BaFe_{0.9-x}Y_{0.1}Co_xO_{3-\delta}$ for x=0 (red line and squares) and 0.15 (blue line and triangles)

Figure 8 Temperature dependence of the inverse molar magnetic susceptibility of (a) $BaFe_{0.85}Y_{0.1}Co_{0.05}O_{3-\delta}$ and (b) $BaFe_{0.75}Y_{0.1}Co_{0.15}O_{3-\delta}$

Figure 9 Thermal expansion of $BaFe_{0.9-x}Y_{0.1}Co_xO_{3-\delta}$ (x=0, 0.05, 0.1, 0.15) samples in air. The inset shows the temperature dependence of the thermal expansion coefficient of $BaFe_{0.8}Y_{0.1}Co_{0.1}O_{3-\delta}$

Figure 10 Room-temperature X-ray diffraction patterns of $BaFe_{0.8}Y_{0.1}Co_{0.1}O_{3-\delta}$ after firing in air (a) in contact with $Ce_{0.8}Sm_{0.2}O_{2-\delta}$ at 1273 K and 1373 K and (b) in contact with $Zr_{0.85}Y_{0.15}O_{2-\delta}$ at 1073 K and 1173 K.

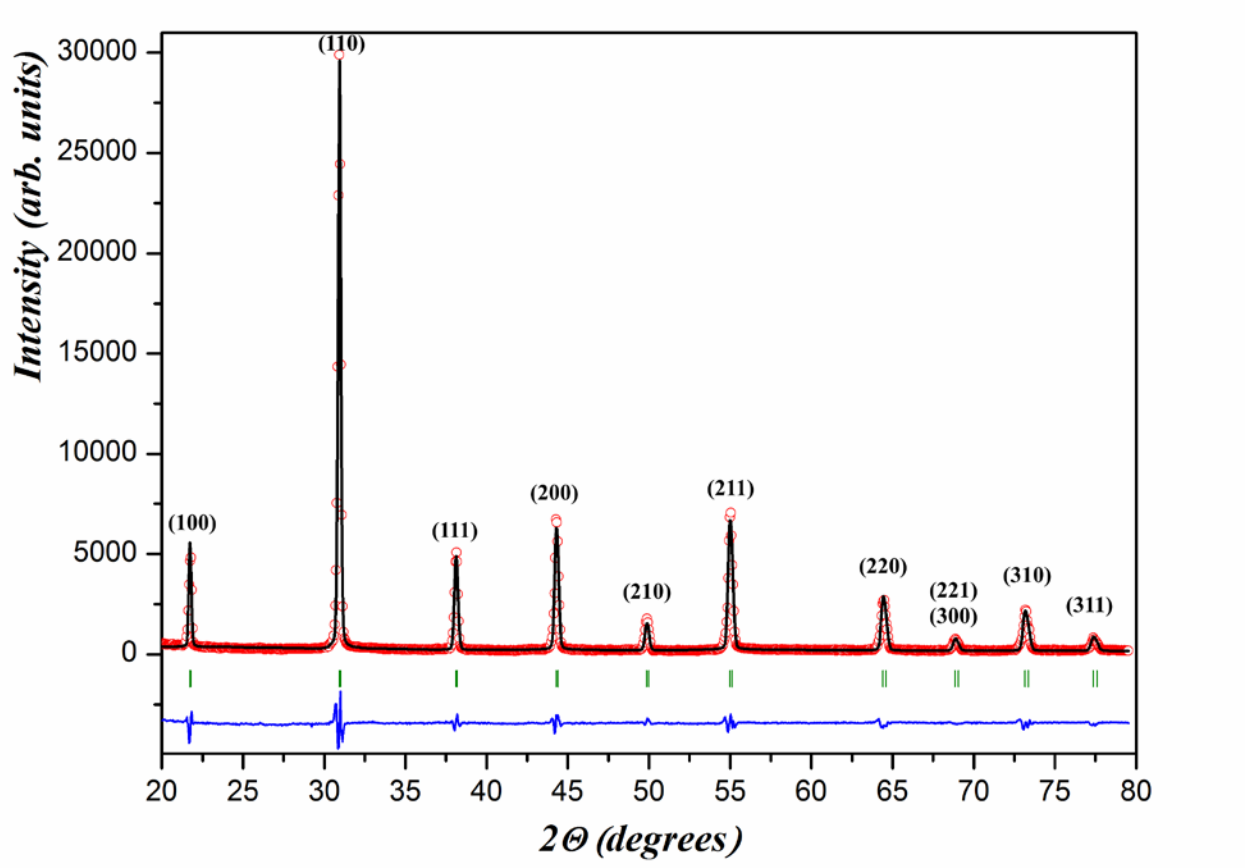

Figure 1

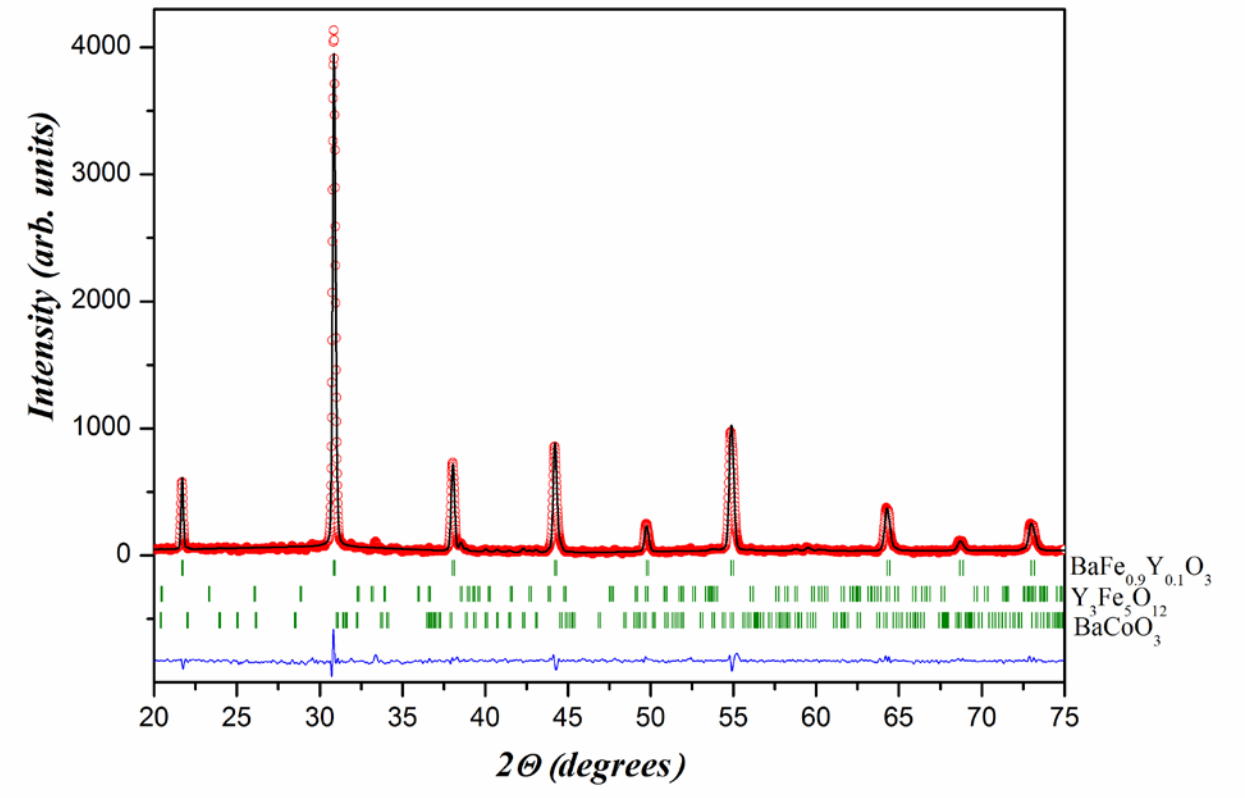

Figure 2

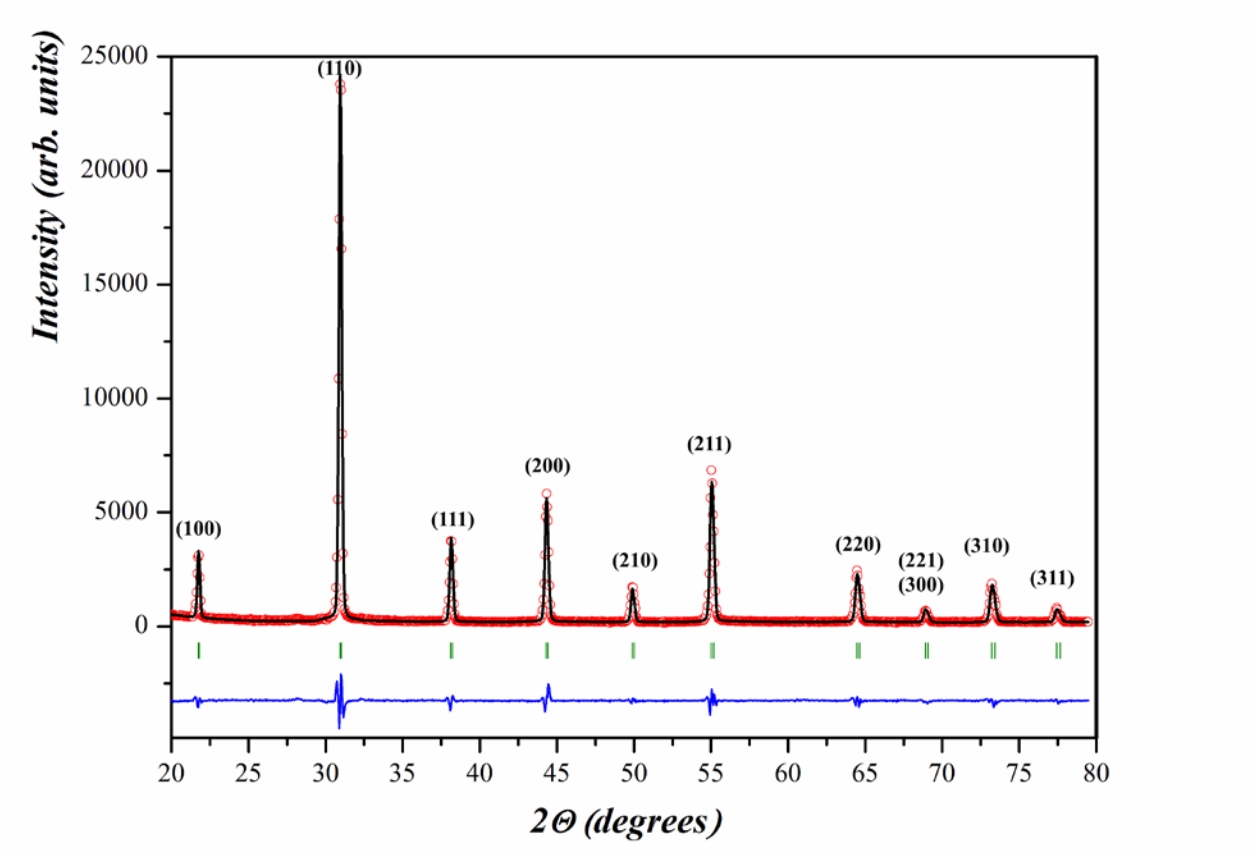

Figure 3

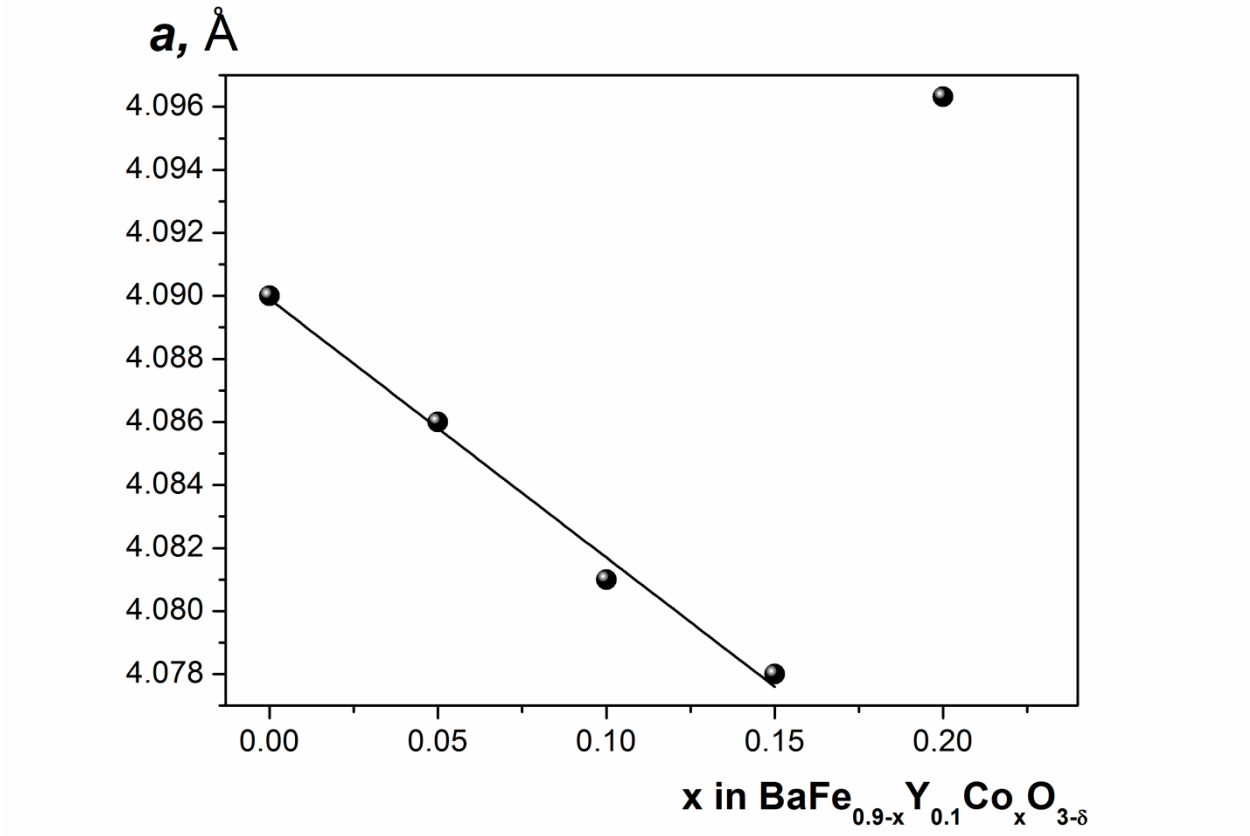

Figure 4

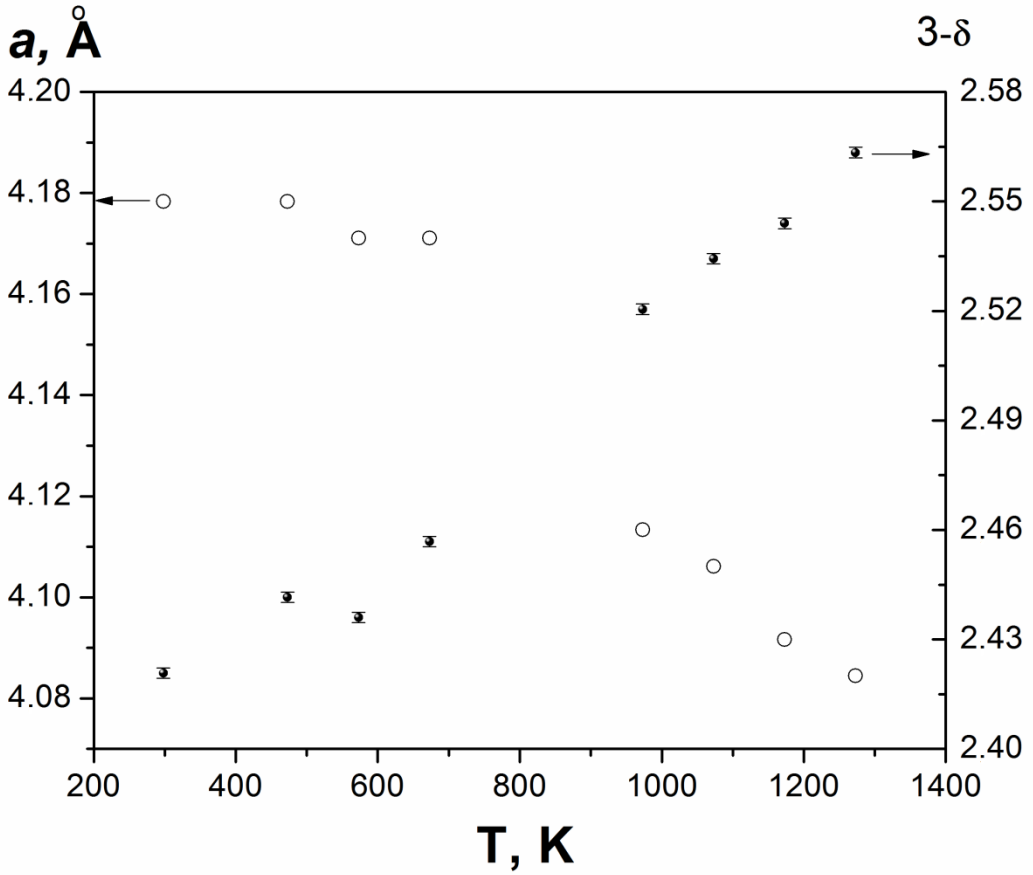

Figure 5

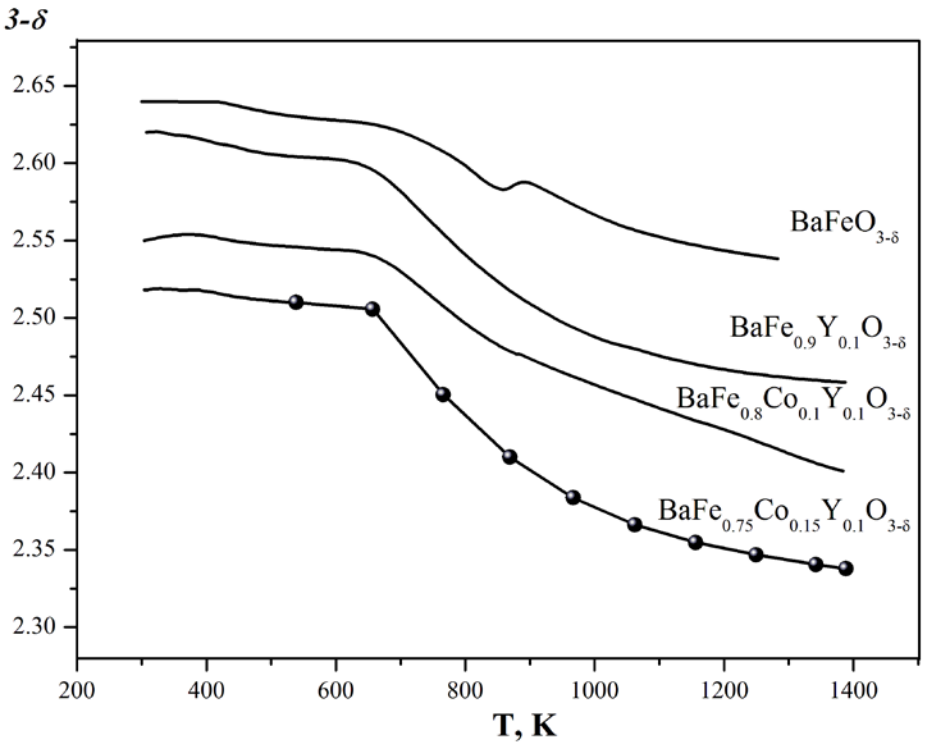

Figure 6

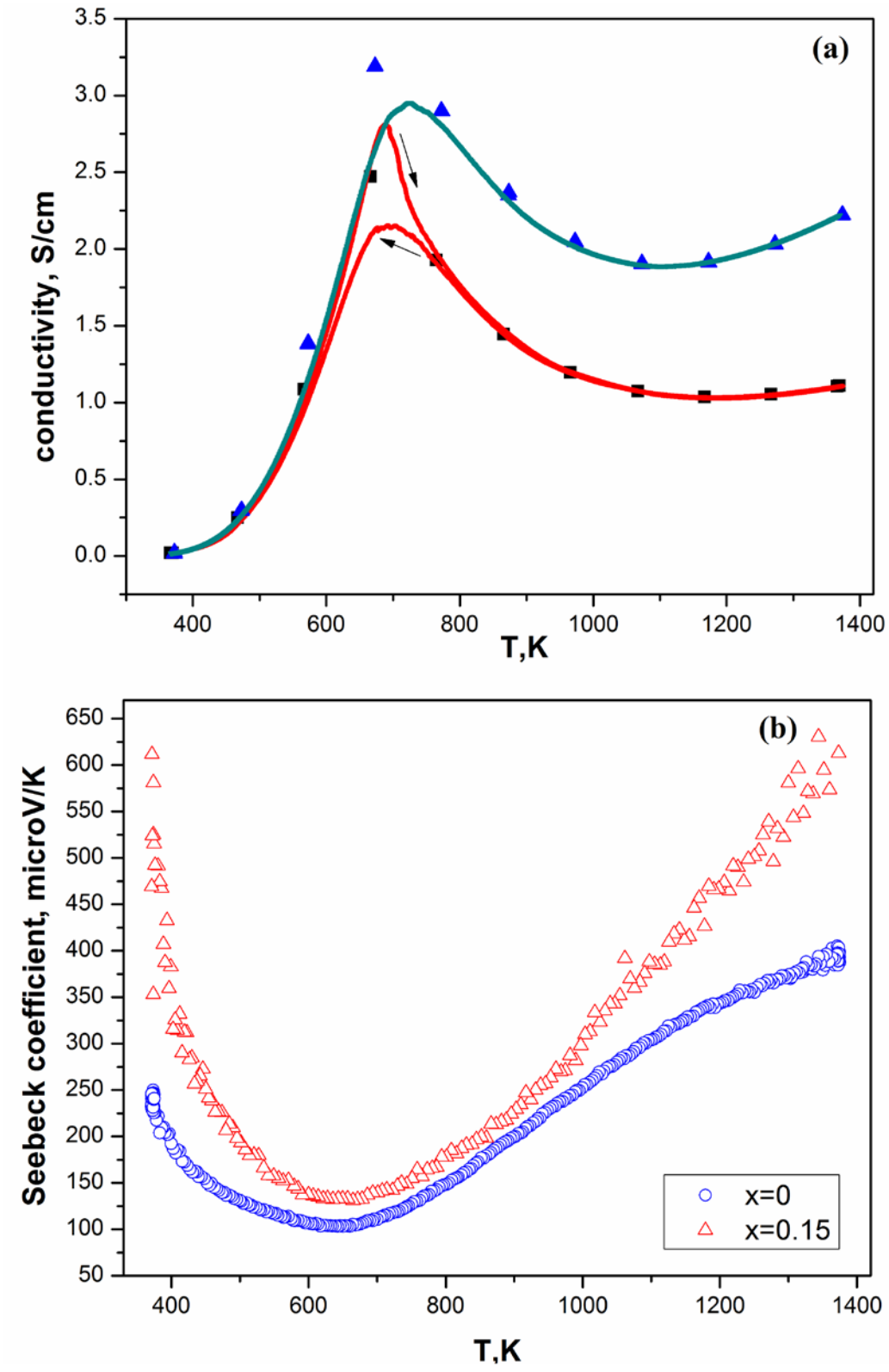
(a)
conductivity, S/cm
T,K
(b)
Seebeck coefficient, microV/K
T,K
x=0
x=0.15

Figure 7

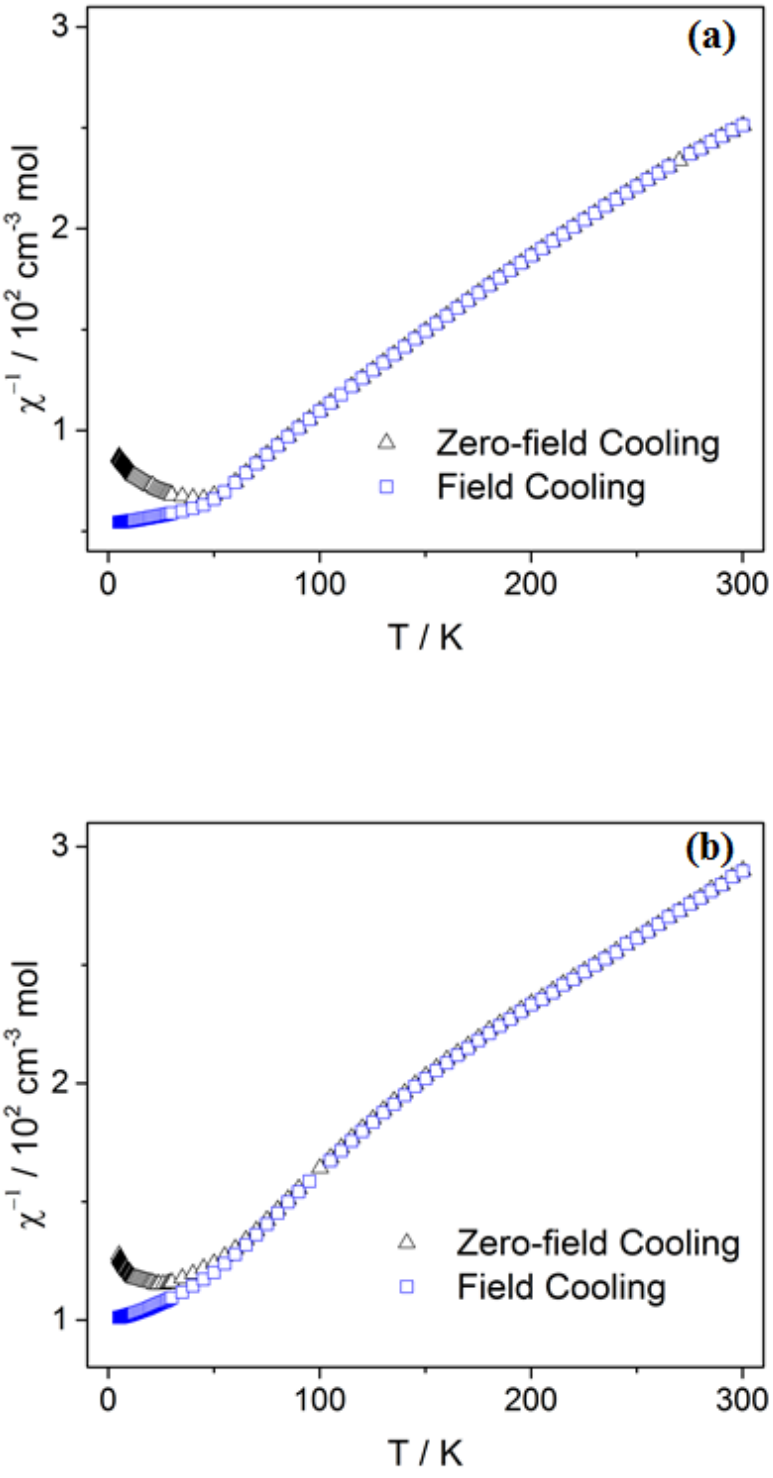
(a)
(b)
χ^{-1} / 10^2 cm^{-3} mol
T / K
Zero-field Cooling
Field Cooling
0
100
200
300
1
2
3

Figure 8

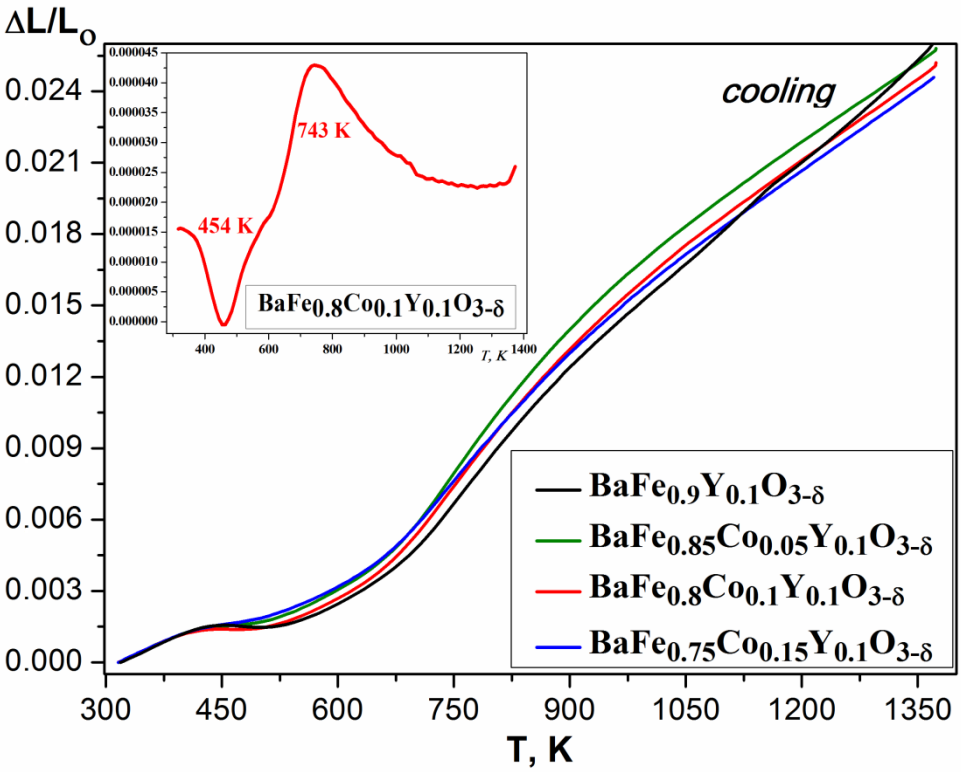
ΔL/L$_o$
0.024
0.021
0.018
0.015
0.012
0.009
0.006
0.003
0.000
300
450
600
750
900
1050
1200
1350
T, K
cooling
743 K
454 K
BaFe$_{0.8}$Co$_{0.1}$Y$_{0.1}$O$_{3-δ}$
T, K
BaFe$_{0.9}$Y$_{0.1}$O$_{3-δ}$
BaFe$_{0.85}$Co$_{0.05}$Y$_{0.1}$O$_{3-δ}$
BaFe$_{0.8}$Co$_{0.1}$Y$_{0.1}$O$_{3-δ}$
BaFe$_{0.75}$Co$_{0.15}$Y$_{0.1}$O$_{3-δ}$

Figure 9

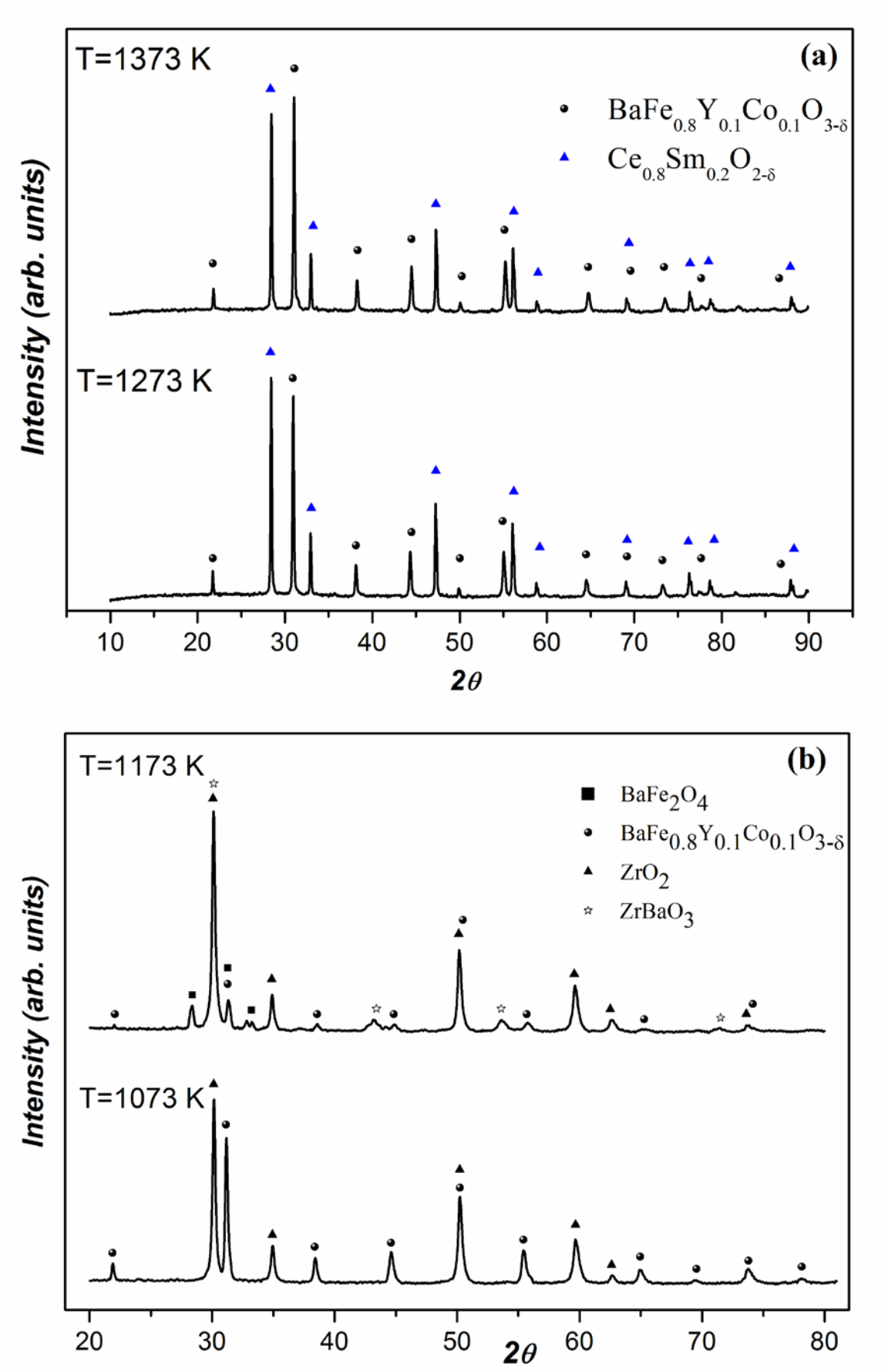
T=1373 K
(a)
BaFe0.8Y0.1Co0.1O3-δ
Ce0.8Sm0.2O2-δ
T=1273 K
Intensity (arb. units)
10
20
30
40
50
60
70
80
90
2θ
T=1173 K
(b)
BaFe2O4
BaFe0.8Y0.1Co0.1O3-δ
ZrO2
ZrBaO3
T=1073 K
Intensity (arb. units)
20
30
40
50
60
70
80
2θ

Figure 10